

Light-Induced Coalescence of Plasmonic Dimers and Clusters

Andrew R. Salmon,[§] Marie-Elena Kleemann,[§] Junyang Huang, William M Deacon, Cloudy Carnegie, Marlous Kamp, Bart de Nijs, Angela Demetriadou, and Jeremy J. Baumberg*



Cite This: <https://dx.doi.org/10.1021/acsnano.0c01213>



Read Online

ACCESS |



Metrics & More



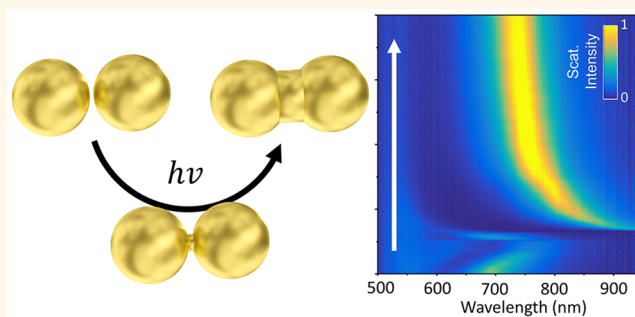
Article Recommendations



Supporting Information

ABSTRACT: The properties of nanoplasmonic structures depend strongly on their geometry, creating the need for high-precision control and characterization. Here, by exploiting the low activation energy of gold atoms on nanoparticle surfaces, we show how laser irradiation reshapes nanoparticle dimers. Time-course dark-field microspectroscopy allows this process to be studied in detail for individual nanostructures. Three regimes are identified: facet growth, formation of a conductive bridge between particles, and bridge growth. Electromagnetic simulations confirm the growth dynamics and allow measurement of bridge diameter, found to be highly reproducible and also self-limiting. Correlations in spectral resonances for the initial and final states give insight into the energy barriers for bridge growth. Dark-field microscopy shows that coalescence of multiple gaps in nanoparticle clusters can be digitally triggered, with each gap closing after discrete increases in irradiation power. Such control is important for light-induced nanowire formation or trimming of electronic and optoelectronic devices.

KEYWORDS: gold nanoparticles, plasmonics, nanoparticle dimers, nanoparticle coalescence, sintering, optical spectroscopy



The coalescence of nanoparticles has significant commercial importance, being fundamental to sintered nanomaterials.¹ This is of interest for a wide variety of applications from printable transistors^{2,3} to conducting wires and contacts⁴ and is approaching large-scale application in the electronics industry.⁵ Nanoparticle coalescence is also crucial for understanding heterogeneous catalysis. Here, small nanoparticles (<10 nm) are required, and these have a high surface energy making them especially prone to agglomeration.^{6,7} Since catalytic activity is critically dependent on the nanoparticle surface area, understanding and preventing agglomeration is crucial.

Studies of nanoparticle sintering take one of two approaches, using electron microscopy⁸ or molecular dynamics simulations,⁹ both of which have limitations. Electron microscopy explores only small sample populations and suffers degradation from the electron beam, while molecular dynamics simulations are limited by computational expense to small nanoparticles.

Here, we study the light-induced bridging of gold nanoparticle (AuNP) dimers by time-resolved optical spectroscopy. This gives highly detailed information as the plasmonic modes are extremely sensitive to the nanoscale geometry. A sequence of structural dynamics is reliably observed: first the contact area between the particles grows, then a conductive filament

fleeting forms across the gap, which finally grows to fill the full contact area, ultimately becoming a large proportion of the nanoparticle diameter. We then extend this analysis to gold nanoparticle clusters and find that the bridging of interparticle gaps occurs digitally, with each coalescence event distinct in the spectral response.

RESULTS AND DISCUSSION

The AuNP dimers are prepared by triggering and then quenching the aggregation of colloidal gold NPs of 70 ± 3 nm diameter. The binding ligand cucurbit[7]uril (CB[7]) is used to initiate the aggregation, which glues the AuNPs together in a diffusion limited process, while also defining the gap size to be 0.9 nm.¹⁰ The aggregation in solution is monitored using extinction spectroscopy (Figure 1a) and abruptly stopped after $t = 9$ s by adding a portion of a melted aqueous 3 wt % agarose

Received: February 11, 2020

Accepted: March 25, 2020

Published: March 25, 2020

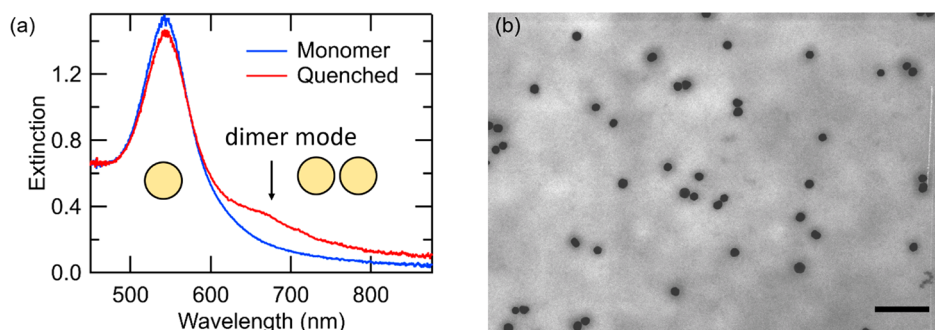


Figure 1. Dimer preparation. (a) Extinction spectra of 70 nm diameter AuNP aqueous suspensions. Cucurbit[7]uril initiates assembly which is then quenched after $t = 9$ s through addition of agarose. This results in a stable mixture of monomers and dimers. (b) Typical scanning transmission micrograph of the quenched suspension (additional micrographs in Figure S1). Scale bar is 500 nm.

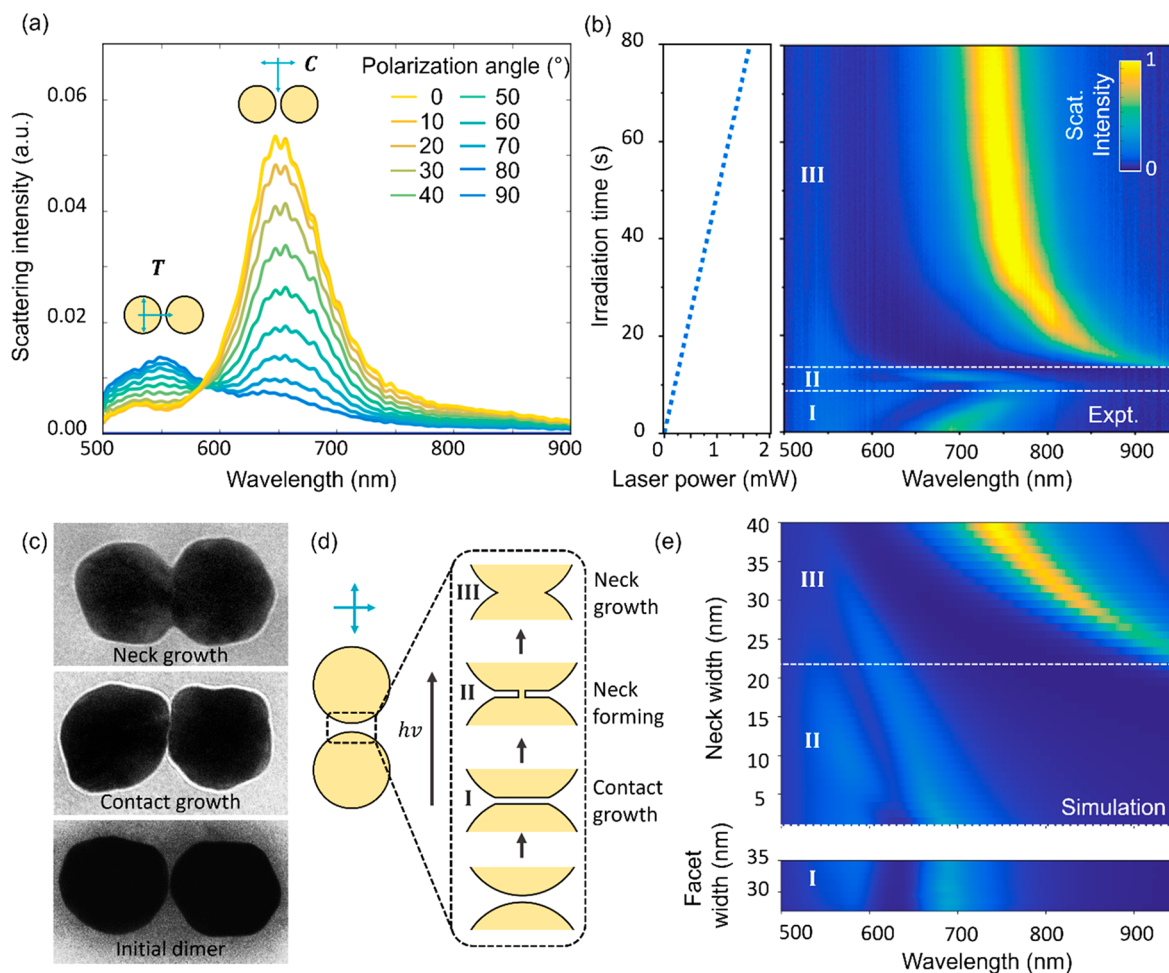


Figure 2. Irradiation of a typical nanoparticle dimer. (a) Polarization-dependent dark-field scattering spectra reveal orientation of dimer axis. (b) Subsequent dark-field scattering spectra during irradiation as a function of laser power (shown to left). (c) Transmission electron micrographs of dimers at different stages of coalescence (corresponding spectra in Figure S3). (d) Schematic of the optically identifiable growth stages (I–III) during irradiation. (e) Simulation of dimer during facet growth (I) and then neck growth (II, III).

solution. The agarose binds to the surface of the AuNPs and quenches the aggregation by restoring the colloidal stability.¹¹ The aggregation quenching is confirmed by the stability of the plasmonic modes in extinction spectroscopy. Using a sealed vial to prevent evaporation, the resulting dimer suspension is stable for weeks.

The number yield of dimers is found to be 26% by TEM, with 4% larger aggregates and 70% monomers ($N = 100$). This is consistent with that expected in the initial stages of diffusion

limited aggregation.¹² The assembly can be quenched at any time to give the corresponding distribution of structures (Figure S1).

For single nanostructure spectroscopy the dimer suspension is drop-cast onto a glass coverslip. Microspectroscopy is performed using a custom-built dark-field microscope with confocal fiber spectral collection. Illumination from a white light laser provides the high intensity illumination required for

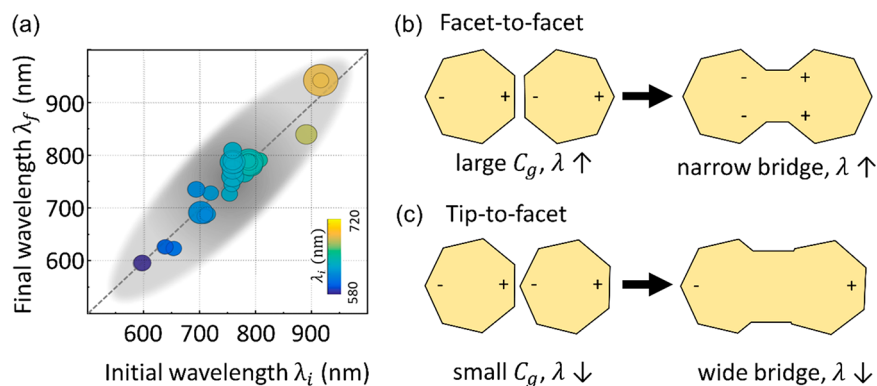


Figure 3. Dependence of charge transfer plasmon on initial contact geometry. (a) Correlation of the initial bonding dipolar mode and the final charge transfer mode. (b, c) Initial and final bridging topology in the case of initially facet-to-facet (b) or tip-to-facet (c) morphologies, showing relation between initial gap capacitance C_g and the final bridge width. The BDP (initial) and CTP (final) modes are indicated.

millisecond scattering spectroscopy on individual nanostructures.

Polarization scans are carried out to distinguish between single nanoparticles and dimers (Figure 2a). The scattering response of dimers has a sinusoidal dependence on the incident polarization angle. The transverse and coupled modes are observed with the polarization perpendicular/parallel to the dimer axis.

In order to study the nanoparticle coalescence, dimers are simultaneously illuminated with a 404 nm laser focused onto the junction by a $\times 63$ imaging objective. The laser is strongly absorbed at this wavelength by the gold interband transition. The dynamical shifts of the optical modes are clearly seen in a representative irradiated nanoparticle dimer (Figure 2b, others in SI). The 404 nm laser power is steadily ramped from 0 to 2 mW (at sample) in steps of 25 μ W. Using 404 nm irradiation to induce coalescence is advantageous because it allows for dark-field scattering spectra to be recorded simultaneously, with a long pass filter to block the laser light. Spectra are taken with an integration time of 100 ms.

It is instructive to estimate the temperature of the dimers for this irradiation. With a 500 nm spot size and an absorption cross section of 10^4 nm² the absorbed power at maximum laser intensity is $P \sim 0.01$ mW. The increase in particle temperature is given by $\delta T = P/(4\pi\kappa R)$ where R is the nanoparticle radius and κ the thermal conductivity of the surrounding medium.¹³ We note this ignores the thermal conduction characteristics of the dimer geometry. While the dimer temperature is thus expected to increase by several hundred degrees, sufficient to cause significant mobility of the surface gold; this is not sufficient to cause a full bulk melting (which indeed is not observed).¹⁴ These temperatures are high enough to decompose organic linkers; consequently the phenomenology is not specific to the CB[7] spacers used. Since the illumination is continuous wave, the heat is uniformly distributed within the particles,¹⁵ contrasting with the case of pulsed illumination where heat is strongly localized according to the optical field profile.¹⁶

For low laser powers, an initial red shift of the coupled mode is seen (stage I, Figure 2b). This is caused by facet growth, which increases the gap capacitance C_g and consequently redshifts the coupled mode.¹⁷ In this phase, surface Au atoms move to lower energy through strong van der Waals attraction to the opposite NP.⁸

At higher laser powers the red shift rate slows and is followed by a rapid blue shift at a critical laser power threshold (stage II). Depending on the individual dimer, multiple blue shifts can occur progressively during stage II (Figure S4). Evidently this stage is strongly dependent on the dimer morphology. Simulations indeed show that additional blue-shifting modes appear if the bridge is off center (Figure S5). The coupled mode blueshift is expected from conductive bridging across the nanoparticle gap, because charge transfer between the nanoparticles reduces the gap capacitance. This shorted coupled mode can equivalently be considered as the second-order charge transfer plasmon. Bridge mode anticrossings are also seen, indicating their interaction with cavity modes as previously reported for the nanoparticle-on-mirror geometry.¹⁹ The bridging modes all show comparably narrow line widths and low scattering strength, suggesting lower coupling efficiencies into the far-field due to their tight confinement.

The final irradiation stage (stage III) is accompanied by the appearance of a high intensity mode approaching from the infrared. This mode corresponds to the charge transfer plasmon (CTP). The frequency of this mode is strongly dependent on the bridge width because it controls the charge/electron transfer from one NP to the other. For narrow bridges, the charge transfer between the nanoparticle gives rise to charges localized/accumulated at the crevice either side of the bridge.²⁰ As the bridge width increases, the coupling at the crevice decreases, causing a blueshift into the visible. We emphasize that the spectral sequence I–III occurs very similarly in many dimers (Figure S4). Additionally, related behavior has been seen previously in the nanoparticle-on-mirror geometry and with silver nanoparticles.¹⁷ This optical phenomenology is a general property of bridging across plasmonic coupled gaps and not particular to the system studied here.

Intriguingly, we find that the final CTP mode blueshifts but only until it reaches the spectral region around the initial bonding dipolar plasmon (BDP) mode λ_i . Higher laser powers up to 2 mW do not initiate further blue or red shifts. Instead, the system remains stable at final wavelength λ_f . Irradiating many different nanoparticle dimers ($N = 32$) gives very consistent behavior, with a strong correlation between the initial bonding dipolar plasmon and the final CTP mode wavelengths (Figure 3a, Figure S4). The wide range of initial spectral positions is typical for such nanoparticle dimers, and

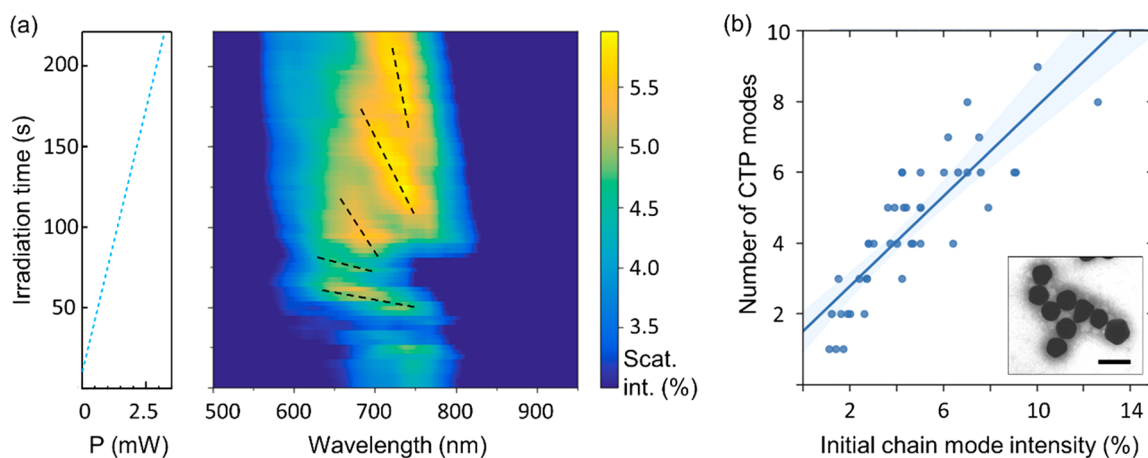


Figure 4. Laser-induced coalescence of typical AuNP cluster. (a) Unpolarized dark-field scattering spectra during irradiation as a function of laser power. Charge transfer plasmon (CTP) modes are indicated (dashed lines). (b) Correlation of number of CTP modes observed with the chain mode scattering intensity before laser irradiation. Inset is a scanning transmission electron micrograph of a typical cluster, scale bar 100 nm.

has been ascribed to the range of different facet alignments between the NPs.²¹ It is important to consider the other factors that can affect the BDP wavelength. The nanoparticle polydispersity is low (4%) and so cannot result in ~ 300 nm shifts of the coupled mode (Figure 3a). Likewise the gap size is well-defined by the CB[7] spacer.¹⁰ Consequently, the contact geometry is indeed the main factor affecting the BDP wavelength.

A strong correspondence between the BDP mode before contact and CTP mode after contact has been predicted previously in simulations on rod dimers.²² In that work, it was found that the correlation is observed for the approach of flat ended rods, but not for rods with hemispherical ends. This result emerges because for both a strongly coupled gap (large capacitance C_g) and for a wide physical contact (low inductance) the dimer is effectively short-circuited and the antenna dipole is equivalent. This can explain why large C_g dimers should have similar spectral resonances in initial and final states. However, the same does not account for a correlation between the initial and final spectral modes of small C_g (e.g., tip-to-facet) dimers. We emphasize that the most obvious explanation, that larger gap contacts generate wider bridges, completely fails as this would give a reversal of the dependence seen in Figure 3a.

The only explanation that accounts for this behavior is if the tip-to-facet geometry (Figure 3d) enhances the ability of the bridge to laterally expand. A wider bridge has two complementary effects. First, wider bridges generate larger crevice dihedral angles. This reduces the localization of the CTP mode to the crevice and causes it to blueshift (Figure 3b,c).²² Second, the preservation of total volume leads to a shortening of the length of the bridged dimer, again blueshifting the CTP mode. This would account for the correlation seen in Figure 3a.

The remaining question is why small C_g contacts result in wider bridges. In general, coalescence is favored because this reduces the surface area and so reduces the surface energy. However, it is common for bridge growth to replace lower energy facets with higher energy facets, which results in the process being kinetically trapped.²³ Molecular dynamics simulations have described how there can be two distinct bonding pathways for gold nanoparticles.²⁴ Above a critical

crystallographic misorientation angle (15° for 10 nm AuNPs) high energy defects are formed during coalescence. It is thus likely that the difference between the coalescence of facet-to-facet and misoriented (e.g., tip-to-facet) contacts is that the latter is a defect-mediated process. We posit that bridge growth allows for these defects to restructure and lower in energy, providing an additional thermodynamic drive for the coalescence process of misoriented dimers and delaying the kinetic trapping.

Optical spectroscopy thus provides significant insight into the coalescence of nanoparticle dimers and is less invasive than typical electron microscopy. Such dimers form the simplest model system and so provide a platform to develop and test coalescence and optical models. However, for many applications it is also necessary to gain understanding beyond this model system to nanoparticle clusters and films. It is thus of interest to examine if our optical analysis extends to larger clusters.

We start by using a similar quenched aggregation to deposit larger gold nanoparticle clusters on glass by delaying the quenching to $t = 30$ s (Figure 4a). We follow the same ramped irradiation protocol and track the optical spectra during the resulting coalescence of different gaps within the cluster (Figure 4a). During light-induced bridging, multiple CTP modes are observed to blueshift into the visible region. This contrasts with the case of dimers where only one CTP mode is seen consistently. We therefore assign this to coalescence across different AuNP contact junctions, which occur at slightly different laser powers depending on their gap geometries, optical in-coupling efficiencies, and local temperatures from different thermal conductive contacts. Consistent with this we find that the number of distinct CTP modes is positively correlated with the scattering intensity (Figure 4b). Larger clusters both scatter more light and have more nanoparticle contact junctions.

The characteristic trends seen in the evolution of successive CTP modes can be considered in terms of excitations of nanoparticle chain subunits.²⁵ Each CTP mode progressively saturates to less blue-shifted wavelengths (Figure 4a) which is caused by the formation of increasingly long fused nanoparticle chains during coalescence. Longer fused chains have a redder longitudinal CTP mode, resembling longer nanorods. The

scattering intensity of the CTP modes also increases because longer fused chains have a larger scattering cross-section.

Simulations show that close to the interband transition NP chain temperatures are highest in the chain center.²⁶ Hence, we expect bridging to occur successively outward from the centers of chains embedded within the clusters. What is apparent is that each bridging appears to be individually identifiable, showing that coalescence does not trigger a runaway process where all bridges form rapidly after the first. This then enables intriguing possibilities, such as the wiring up of well-defined electronic contacts from aggregates which are illuminated to control the electrical transport through the tunneling gaps. Further work assembling such aggregates on contacts is thus of interest.

CONCLUSIONS

In summary, the plasmonic response of nanoparticle dimers and clusters during laser-induced coalescence reveals three distinct processes. First, the facet area between a dimer grows, second, a thin conductive bridge connects the particles, and third, the bridge grows broader and ultimately becomes a large proportion of the nanoparticle diameter. A strong correlation is observed between the initial BDP and final CTP modes, indicating a correlation between the initial contact geometry and the width of the bridge. Dark-field spectroscopy on AuNP clusters also reveals the coalescence of individual nanoparticle junctions resulting in multiple distinct CTP modes, which can be successively triggered. This is relevant for the optical writing of open/closed gaps in electronic devices as well as light-trimmed antenna structures for coupling to nanoscale dipole emitters in the gaps.

EXPERIMENTAL METHODS

Gold Nanoparticles. Gold nanoparticles were made in a three-step seeded synthesis following the method of Ziegler *et al.*²⁷ These were characterized by scanning transmission electron microscopy (Hitachi S-5500), with a diameter of 70 ± 3 nm (standard deviation) from 100 measurements. Dimers were prepared by a quenched aggregation. A 20 μ L portion of 1 mg/mL of cucurbit[7]uril was added to 500 μ L of the gold nanoparticle suspension to initiate aggregation. At an appropriate time (~ 9 s for dimers, ~ 30 s for clusters) the aggregation was quenched through the addition of 10 μ L of a melted 3 wt % agarose gel. These were then drop cast onto glass slides for spectroscopy.

For correlation of TEM and optical spectroscopy, the dimers were cast onto SiN TEM windows (Agar Scientific, S172-4T, 100 nm membrane thickness).

Optical Microscopy and Spectroscopy. Optical microscopy and spectroscopy was performed using a custom-built dark-field microscope.²⁸ In order to achieve sufficient signal for high time-resolution measurements on dimers, illumination is from a white light laser (Fianium SC400-4). A Leica 63 \times 1.2NA water immersion objective was used. Spectra are taken using a fiber-coupled and a cooled Ocean Optics spectrometer (QE Pro). Spectra are referenced using a white light scattering standard (Labsphere Spectralon SRM 99).

Simulations. The electromagnetic response of the dimer geometries is simulated by three-dimensional finite-difference time-domain (FDTD) calculations using Lumerical FDTD Solutions. For dimer merging, the AuNPs are modeled as two merged ellipsoids keeping the length, width, and volume constant as the morphology of the nanoparticles changes. The optical properties are fitted to Johnson and Christy experimental data for gold. The CB[7] spacer layer is modeled as a uniform coating around the particle surface with thickness of 0.9 nm and refractive index of $n = 1.4$. The SiO₂ substrate was confirmed to have a negligible impact on the spectra by

simulations and was therefore excluded. The system is illuminated with a plane wave polarized parallel to the dimer axis.

ASSOCIATED CONTENT

Supporting Information

The Supporting Information is available free of charge at <https://pubs.acs.org/doi/10.1021/acsnano.0c01213>.

Additional STEM images, spectra of assembly quenching at a series of times, additional dimer coalescence time-series spectra, spectra of partially fused dimers and corresponding TEMs, and FDTD simulations of asymmetric bridging and bridging with differing initial contact angles (PDF)

AUTHOR INFORMATION

Corresponding Author

Jeremy J. Baumberg – Nanophotonics Centre, Cavendish Laboratory, University of Cambridge, Cambridge CB3 0HE, United Kingdom; orcid.org/0000-0002-9606-9488; Email: jjb12@cam.ac.uk

Authors

Andrew R. Salmon – Nanophotonics Centre, Cavendish Laboratory, University of Cambridge, Cambridge CB3 0HE, United Kingdom; orcid.org/0000-0001-6267-5896

Marie-Elena Kleemann – Nanophotonics Centre, Cavendish Laboratory, University of Cambridge, Cambridge CB3 0HE, United Kingdom

Junyung Huang – Nanophotonics Centre, Cavendish Laboratory, University of Cambridge, Cambridge CB3 0HE, United Kingdom

William M Deacon – Nanophotonics Centre, Cavendish Laboratory, University of Cambridge, Cambridge CB3 0HE, United Kingdom

Cloudy Carnegie – Nanophotonics Centre, Cavendish Laboratory, University of Cambridge, Cambridge CB3 0HE, United Kingdom

Marlous Kamp – Nanophotonics Centre, Cavendish Laboratory, University of Cambridge, Cambridge CB3 0HE, United Kingdom

Bart de Nijs – Nanophotonics Centre, Cavendish Laboratory, University of Cambridge, Cambridge CB3 0HE, United Kingdom

Angela Demetriadou – School of Physics and Astronomy, University of Birmingham, Birmingham B15 2TT, United Kingdom; orcid.org/0000-0001-7240-597X

Complete contact information is available at: <https://pubs.acs.org/10.1021/acsnano.0c01213>

Author Contributions

[§]A.R.S. and M.-E.K. contributed equally.

Notes

The authors declare no competing financial interest.

The spectroscopic data used for analysis in this publication are available at <https://doi.org/10.17863/CAM.S0893>.

ACKNOWLEDGMENTS

We acknowledge UK EPSRC grants EP/L027151/1 and EU 778616 ANTNAME. B.d.N. acknowledges support from the Leverhulme Trust and Isaac Newton Trust in the form of an ECF; B.d.N. and M.K. acknowledge the Winton Programme for the Physics of Sustainability. M.K. is grateful to the

European Commission for a Marie Curie fellowship (grant 7020005, SPARCLES). A.D. acknowledges support from the Royal Society URF\180097 and RGF\EA\181038.

REFERENCES

- (1) Liu, W.; An, R.; Wang, C.; Zheng, Z.; Tian, Y.; Xu, R.; Wang, Z. Recent Progress in Rapid Sintering of Nanosilver for Electronics Applications. *Micromachines* **2018**, *9*, 346.
- (2) Ko, S. H.; Pan, H.; Grigoropoulos, C. P.; Luscombe, C. K.; Fréchet, J. M. J.; Poulidakos, D. Air Stable High Resolution Organic Transistors by Selective Laser Sintering of Ink-Jet Printed Metal Nanoparticles. *Appl. Phys. Lett.* **2007**, *90*, 141103.
- (3) Zhao, N.; Chiesa, M.; Sirringhaus, H.; Li, Y.; Wu, Y.; Ong, B. Self-Aligned Inkjet Printing of Highly Conducting Gold Electrodes with Submicron Resolution. *J. Appl. Phys.* **2007**, *101*, 064513.
- (4) Ko, S. H.; Pan, H.; Grigoropoulos, C. P.; Luscombe, C. K.; Fréchet, J. M. J.; Poulidakos, D. All-Inkjet-Printed Flexible Electronics Fabrication on a Polymer Substrate by Low-Temperature High-Resolution Selective Laser Sintering of Metal Nanoparticles. *Nanotechnology* **2007**, *18*, 345202.
- (5) Siow, K. S.; Lin, Y. T. Identifying the Development State of Sintered Silver (Ag) as a Bonding Material in the Microelectronic Packaging via a Patent Landscape Study. *J. Electron. Packag.* **2016**, *138*, 020804.
- (6) Asoro, M. A.; Kovar, D.; Shao-Horn, Y.; Allard, L. F.; Ferreira, P. J. Coalescence and Sintering of Pt Nanoparticles: *In Situ* Observation by Aberration-Corrected HAADF STEM. *Nanotechnology* **2010**, *21*, 025701.
- (7) Liu, L.; Corma, A. Metal Catalysts for Heterogeneous Catalysis: From Single Atoms to Nanoclusters and Nanoparticles. *Chem. Rev.* **2018**, *118*, 4981–5079.
- (8) Li, D.; Nielsen, M. H. M. H.; Lee, J. R. I. J. R. I.; Frandsen, C.; Banfield, J. F.; De Yoreo, J. J. Direction-Specific Interactions Control Crystal Growth by Oriented Attachment. *Science* **2012**, *336*, 1014–1018.
- (9) Grammatikopoulos, P.; Sowwan, M.; Kioseoglou, J. Computational Modeling of Nanoparticle Coalescence. *Adv. Theory Simulations* **2019**, *2*, 1900013.
- (10) Taylor, R. W.; Lee, T.-C.; Scherman, O. A.; Esteban, R.; Aizpurua, J.; Huang, F. M.; Baumberg, J. J.; Mahajan, S. Precise Subnanometer Plasmonic Junctions for SERS within Gold Nanoparticle Assemblies Using Cucurbit[n]Urils “Glue”. *ACS Nano* **2011**, *5*, 3878–3887.
- (11) Kattumuri, V.; Chandrasekhar, M.; Guha, S.; Raghuraman, K.; Katti, K. V.; Ghosh, K.; Patel, R. J. Agarose-Stabilized Gold Nanoparticles for Surface-Enhanced Raman Spectroscopic Detection of DNA Nucleosides. *Appl. Phys. Lett.* **2006**, *88*, 153114.
- (12) Salmon, A. R.; Esteban, R.; Taylor, R. W.; Hugall, J. T.; Smith, C. A.; Whyte, G.; Scherman, O. A.; Aizpurua, J.; Abell, C.; Baumberg, J. J. Monitoring Early-Stage Nanoparticle Assembly in Microdroplets by Optical Spectroscopy and SERS. *Small* **2016**, *12*, 1788–1796.
- (13) Baffou, G.; Quidant, R. Nanoplasmonics for Chemistry. *Chem. Soc. Rev.* **2014**, *43*, 3898–3907.
- (14) Barnard, A. S.; Young, N. P.; Kirkland, A. I.; Van Huis, M. A.; Xu, H. Nanogold: A Quantitative Phase Map. *ACS Nano* **2009**, *3*, 1431–1436.
- (15) Baffou, G.; Quidant, R. Thermo-Plasmonics: Using Metallic Nanostructures as Nano-Sources of Heat. *Laser Photonics Rev.* **2013**, *7*, 171–187.
- (16) González-Rubio, G.; González-Izquierdo, J.; Bañares, L.; Tardajos, G.; Rivera, A.; Altantzis, T.; Bals, S.; Peña-Rodríguez, O.; Guerrero-Martínez, A.; Liz-Marzán, L. M. Femtosecond Laser-Controlled Tip-To-Tip Assembly and Welding of Gold Nanorods. *Nano Lett.* **2015**, *15*, 8282–8288.
- (17) Mertens, J.; Demetriadou, A.; Bowman, R. W.; Benz, F.; Kleemann, M. E.; Tserkezis, C.; Shi, Y.; Yang, H. Y.; Hess, O.; Aizpurua, J.; Baumberg, J. J. Tracking Optical Welding through Groove Modes in Plasmonic Nanocavities. *Nano Lett.* **2016**, *16*, 5605–5611.
- (18) Wang, J.; Chen, S.; Cui, K.; Li, D.; Chen, D. Approach and Coalescence of Gold Nanoparticles Driven by Surface Thermodynamic Fluctuations and Atomic Interaction Forces. *ACS Nano* **2016**, *10*, 2893–2902.
- (19) Tserkezis, C.; Esteban, R.; Sigle, D. O.; Mertens, J.; Herrmann, L. O.; Baumberg, J. J.; Aizpurua, J. Hybridization of Plasmonic Antenna and Cavity Modes: Extreme Optics of Nanoparticle-On-Mirror Nanogaps. *Phys. Rev. A: At., Mol., Opt. Phys.* **2015**, *92*, 053811.
- (20) Romero, I.; Aizpurua, J.; Bryant, G. W.; García De Abajo, F. J. Plasmons in Nearly Touching Metallic Nanoparticles: Singular Response in the Limit of Touching Dimers. *Opt. Express* **2006**, *14*, 9988.
- (21) Yoon, J. H.; Selbach, F.; Schumacher, L.; Jose, J.; Schlücker, S. Surface Plasmon Coupling in Dimers of Gold Nanoparticles: Experiment and Theory for Ideal (Spherical) and Nonideal (Faceted) Building Blocks. *ACS Photonics* **2019**, *6*, 642–648.
- (22) Esteban, R.; Aguirregabiria, G.; Borisov, A. G.; Wang, Y. M.; Nordlander, P.; Bryant, G. W.; Aizpurua, J. The Morphology of Narrow Gaps Modifies the Plasmonic Response. *ACS Photonics* **2015**, *2*, 295–305.
- (23) Lange, A. P.; Samanta, A.; Majidi, H.; Mahajan, S.; Ging, J.; Olson, T. Y.; van Benthem, K.; Elhadj, S. Dislocation Mediated Alignment during Metal Nanoparticle Coalescence. *Acta Mater.* **2016**, *120*, 364–378.
- (24) Aabdin, Z.; Lu, J.; Zhu, X.; Anand, U.; Loh, N. D.; Su, H.; Mirsaidov, U. Bonding Pathways of Gold Nanocrystals in Solution. *Nano Lett.* **2014**, *14*, 6639–6643.
- (25) Esteban, R.; Taylor, R. W.; Baumberg, J. J.; Aizpurua, J. How Chain Plasmons Govern the Optical Response in Strongly Interacting Self-Assembled Metallic Clusters of Nanoparticles. *Langmuir* **2012**, *28*, 8881–8890.
- (26) Baffou, G.; Quidant, R.; García De Abajo, F. J. Nanoscale Control of Optical Heating in Complex Plasmonic Systems. *ACS Nano* **2010**, *4*, 709–716.
- (27) Ziegler, C.; Eychmüller, A. Seeded Growth Synthesis of Uniform Gold Nanoparticles with Diameters of 15–300 Nm. *J. Phys. Chem. C* **2011**, *115*, 4502–4506.
- (28) Kleemann, M. E.; Mertens, J.; Zheng, X.; Cormier, S.; Turek, V.; Benz, F.; Chikkaraddy, R.; Deacon, W.; Lombardi, A.; Moshchalkov, V. V.; Vandenbosch, G. A. E.; Baumberg, J. J. Revealing Nanostructures through Plasmon Polarimetry. *ACS Nano* **2017**, *11*, 850–855.